PNAS Nexus, 2024, 3, pgae128
https://doi.org/10.1093/pnasnexus/pgae128
Advance access publication 22 March 2024
Research Report

Custom-designed, mass silk production in genetically engineered silkworms

Ye Yu[a,b], Kai Chen[a,b], Jingxia Wang[c,d], Zhongjie Zhang[a,b], Bo Hu[a,b], Xiaojing Liu[a,b], Zhi Lin[c,d] and Anjiang Tan[a,b,*]

[a]Jiangsu Key Laboratory of Sericultural Biology and Biotechnology, School of Biotechnology, Jiangsu University of Science and Technology, Zhenjiang 212100, China
[b]Key Laboratory of Silkworm and Mulberry Genetic Improvement, Ministry of Agriculture and Rural Affairs, Sericultural Scientific Research Center, Chinese Academy of Agricultural Sciences, Zhenjiang 212100, China
[c]School of Life Sciences, Tianjin University, Tianjin 300072, China
[d]Tianjin Key Laboratory of Function and Application of Biological Macromolecular Structures, School of Life Sciences, Tianjin University, Tianjin 300072, China
*To whom correspondence should be addressed: Email: atan@just.edu.cn
Edited By: Ivet Bahar

Abstract

Genetically engineered silkworms have been widely used to obtain silk with modified characteristics especially by introducing spider silk genes. However, these attempts are still challenging due to limitations in transformation strategies and difficulties in integration of the large DNA fragments. Here, we describe three different transformation strategies in genetically engineered silkworms, including transcription-activator-like effector nuclease (TALEN)-mediated fibroin light chain (FibL) fusion (BmFibL-F), TALEN-mediated FibH replacement (BmFibH-R), and transposon-mediated genetic transformation with the silk gland-specific fibroin heavy chain (FibH) promoter (BmFibH-T). As the result, the yields of exogenous silk proteins, a 160 kDa major ampullate spidroin 2 (MaSp2) from the orb-weaving spider *Nephila clavipes* and a 226 kDa fibroin heavy chain protein (EvFibH) from the bagworm *Eumeta variegate*, reach 51.02 and 64.13% in BmFibH-R transformed cocoon shells, respectively. Moreover, the presence of MaSp2 or EvFibH significantly enhances the toughness of genetically engineered silk fibers by ~86% in BmFibH-T and ~80% in BmFibH-R silkworms, respectively. Structural analysis reveals a substantial ~40% increase in fiber crystallinity, primarily attributed to the presence of unique polyalanines in the repetitive sequences of MaSp2 or EvFibH. In addition, RNA-seq analysis reveals that BmFibH-R system only causes minor impact on the expression of endogenous genes. Our study thus provides insights into developing custom-designed silk production using the genetically engineered silkworm as the bioreactor.

Keywords: genome editing, TALEN, spider silk, *Eumeta variegate*, *Bombyx mori*

Significance Statement

Numerous efforts have attempted to improve mechanical properties of silk fibers via expressing spider silk proteins. However, such studies are still challenging due to limitation of expressing strategies. Here, we describe exogenous silk protein production in genetically modified silkworms by using multiply transformation strategies. Remarkably, through targeted gene replacement, the yield of 160 kDa *Nephila clavipes* major ampullate spidroin 2 (MaSp2) and 226 kDa *Eumeta variegate* fibroin heavy chain protein (EvFibH) can reach up to 51.02 and 64.13% of cocoon shells, respectively. More importantly, the comprehensive mechanical properties of genetically modified silk fibers were sharply improved. This study will pave the way for future custom-designed silk production using *Bombyx mori* as a promising bioreactor.

Introduction

Silks are natural protein fibers synthesized by arthropod, most notably silkworms and spiders (1–3). Silk fibers have attracted both scientific and economic interest in the fields of biology, medical, chemistry, and materials science, owing to their extraordinary mechanical properties, favorable biocompatibility and biodegradability (4–7). The mechanical properties of silk are predominantly determined by the primary structure and condensed state structure of silk protein (7–10). As one of the most excellent silk fibers in nature, spider dragline silk combines high strength and superior extensibility (11–14). The strength of dragline silk from the golden orb-weaver *Nephila clavipes* is comparable with technological materials, such as high-tensile steel and Kevlar (15, 16). Moreover, *N. clavipes* dragline silk shows highly overall toughness, which depends strongly on the extensibility (13, 16–18). The major ampullate spidroin 2 (MaSp2), one of the major compositions of the dragline silk, is proposed to be responsible for the extensibility. MaSp2 consists of regular repetitive motifs and nonrepetitive

Competing Interest: The authors declare no competing interest.
Received: February 13, 2024. **Accepted:** March 14, 2024

regulatory N-terminal and C-terminal domains (NTD and CTD, respectively) (13, 19–21). The repetitive motifs of MaSp2 can be classified into two categories: polyalanine motifs (polyA/GA) and GPGGX (X = typically Y, P, or Q) motifs. The polyA/GA motifs form β-sheet and assemble ordered crystalline region of MaSp2, while the GPGGX motifs are proposed to be involved in β-turn spiral formation, giving rise to the disordered noncrystalline regions of MaSp2 (13, 22–24). Compared with major ampullate spidroin 1 (MaSp1), the spidroin supposed to be implicated in high-tensile strength of silk fiber, MaSp2 is poorly studied (25, 26). The main difference between MaSp1 and MaSp2 lines in the proline content in sequence and polymeric patterns (13, 27). Based on the characteristics of amino acid sequence and block structure, proline-related motif GPGGX is hypothesized to be responsible for the extensibility of the fiber (13, 23, 28).

The bagworm, *Eumeta variegate*, produces silk that combines with plant materials, forming portable bag against natural enemies (29). In recent years, the bagworm silk has been paid great attention due to its superior mechanical properties including extraordinarily high modulus, strength, and excellent tensile deformation behavior (30–32). Previous study reported that the silk from the Darwin's bark spider *Caerostris darwini* is the toughest known biomaterial compared with any previously described silk (33, 34). Surprisingly, the toughness of bagworm silk is even higher than that of *C. darwini* silk. The mechanical properties of bagworm silk are predominantly attributable to the contribution of silk fibroin heavy chain (EvFibH) (31, 32). There are three characteristic motifs, polyA, poly (GA), and GGX in EvFibH amino acid sequence, combining characteristics of that in *Bombyx mori*, spider dragline silk and *Saturniidae* moths, despite several decisive distinctions from their motifs (32–36).

The silk from the domesticated silkworm, *B. mori*, is the only secretory natural protein fiber that be produced and utilized in large scales. Silk from *B. mori* is composed of fibroin proteins coated with adhesive sericin proteins. Fibroins are core fibrous proteins primarily determining mechanical properties of silk fibers. The fibroin is a 2,300 kDa molecular complex consists of the fibroin heavy chain (BmFibH, 350 kDa), the fibroin light chain (BmFibL, 25.8 kDa), and the fibrohexamerin protein (BmP25, 25.7 kDa) with a molar ratio of 6:6:1 (37–39). More importantly, *B. mori* is an ideal bioreactor for expressing exogenous proteins attributing to high capacity for protein synthesis in the silk gland (SG) and the efficient genetic manipulation technology has been established (40–42). Numerous efforts have attempted to improve mechanical properties of silk fibers via expressing spider silk proteins (20, 23, 26). In the previous work, we achieved massive spider silk protein production through performing transcription-activator-like effector nuclease (TALEN)-mediated homology-directed repair to replace the *BmFibH* with partial MaSp1 gene (39). It is also reported that production of spider silk proteins in the silkworm through employing clustered regularly interspaced short-palindromic repeats (CRISPR) and CRISPR-associated protein 9 (CRISPR/Cas9) technology can significantly improve mechanical properties of silk fibers (43, 44). However, such study is still challenging due to limitations in transformation strategies and difficulties in integration of the large DNA fragments.

In the current study, we established comprehensive transformation strategies including TALEN-mediated BmFibL fusion system (BmFibL-F), TALEN-mediated BmFibH replacement system (BmFibH-R) and *piggyBac*-mediated transgenic system (BmFibH-T) in *B. mori*. The presence of the 160 kDa MaSp2 protein significantly enhanced the extensibility of silk fiber in transformed silkworm lines. In comparison, the BmFibH-R system achieved the highest yield of MaSp2 production with minor influence on the silkworm physiology. The RNA-seq analysis also revealed that expression of endogenous genes only slightly affected in BmFibH-R silkworms. We further established two silkworm lines to express the chimeric 226 kDa EvFibH protein and the transformed EvFibH silk fiber showed significantly improved mechanical properties, especially the strength. Notably, the protein expression amount of MaSp2 and EvFibH by using the BmFibH-R system reach unprecedented yield with 51.02 and 64.13%, respectively, in transformed cocoon shells. Our data indicated that MaSp2 and EvFibH were responsible for extensibility and strength of transformed silk fibers, respectively, paving the way for future custom-designed silk production using *B. mori* as a promising bioreactor.

Results

Construction of genetically engineered silkworms expressing MaSp2

To clarify the role of MaSp2 in mechanical properties of silk fiber, we established silkworm lines expressing MaSp2 using three different expressing systems, BmFibL-F, BmFibH-R, and BmFibH-T. *BmFibL* gene consists of seven exons, encoding a protein of 25.8 kDa in molecular weight. To achieve MaSp2 fusion expression with endogenous BmFibL, we designed a pair of TALENs targeting stop codon of *BmFibL* on exon 7 (FL-TALEN) (Fig. 1A). The cleavage efficiency of the TALENs pair was validated using the firefly luciferase single strand annealing recombination assay in mammalian 293T cells, and the luciferase activities of the TALENs constructs were 28.6-fold higher than the control (Fig. S1A and B). For targeted integration, the donor plasmid (*FibL-MaSp2*-Donor) containing 5,871 bp synthetic *MaSp2* coding sequence (CDS), red fluorescent protein DsRed2 expression cassette, ~1 kb homologous left and right arms in length for each was constructed. In addition, the sequence coding self-cleavage peptide 2A was linked with 5′ terminal of *MaSp2* CDS. As the result, *MaSp2* fusion expression was controlled by the native *BmFibL* regulatory elements.

The BmFibH-R system was as previously described (39). In brief, synthetic *MaSp2* CDS was targeted integrated into *BmFibH* locus with the help of two pairs of TALENs (FH-TALEN1 and FH-TALEN2) and the donor plasmid (*FibH-MaSp2*-Donor) (Fig. S1A and C). In BmFibH-R system, expression of the endogenous *BmFibH* was completely silenced and *MaSp2* expression was driven by the native *BmFibH* regulatory elements (Fig. 1B). In BmFibH-T system, *MaSp2* expression was under control of *BmFibH* promoter and regulatory elements N-terminal domain (NTD), and the 180 bp C-terminal domain (CTD). NTD, including 139 bp exon 1, 971 bp intron and a part of the exon 2 (411 bp), is essential for *BmFibH* transcription, while CTD is needed for silk spinning (Fig. 1C).

In all systems, red fluorescent protein2 (DsRed2) driven by the 3 × P3 promoter served as screen marker. We obtained positive transformed silkworms through the germ line transformation as described previously (39, 45) (Fig. S2A). The transformation efficiency of 2.3, 1.3, and 7.4% was defined for each group as the proportion of fertile injection survivors producing one or more transgenic offspring (Table S1). Genotype of the positive transformed animals in *BmFibL-F* and *BmFibH-R* systems were examined through 5′ and 3′-junction PCR followed by Sanger sequencing (Fig. S2B and C). Both ~7.5 kb *L-Sp2-F* and *H-Sp2-R* donors were precisely and seamlessly integrated into the targeted locus. For *H-Sp2-T* lines, we selected one of the four lines for further analysis.

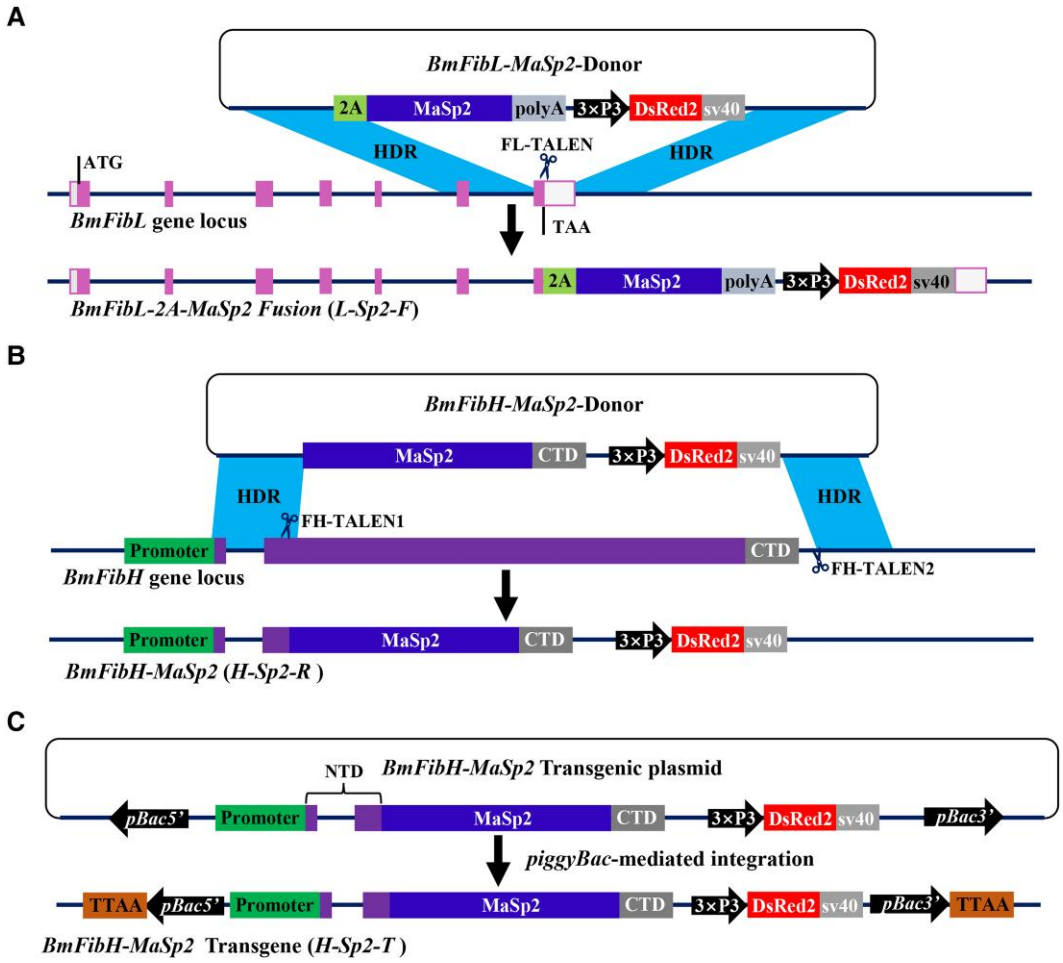

Fig. 1. Schematic representations of three different expressing strategies to achieve MaSp2 expression. A) Schematic representation of the *BmFibL* gene locus and the *FibL-MaSp2*-Donor construct. The hollow boxes represent the UTR, while the solid boxes signify CDSs. The thin line represents genomic and intron DNA. The plasmid FibL-MaSp2-Donor carries CDS of *MaSp2*, which linked with the sequence of self-cleave peptide 2A, and the dominant eye marker gene (3 × DsRed2) cassette inserted between regions of homology from *BmFibL* locus that directly abut FL-TALEN cut site. B) Schematic representation of the *BmFibH* gene locus and the *FibH-MaSp2*-Donor construct. The plasmid *FibH-MaSp2*-Donor comprises CDS of *MaSp2* lined with CTD of *BmFibH* and 3 × DsRed2 cassette, along with homology from *BmFibH* locus that immediately adjacent to 5′ and 3′ ends of FH-TALEN1 and FH-TALEN2 cut sites, respectively. C) Schematic representations of the plasmid constructs for production transgenic silkworms (*H-SP2-T*). Expression of *MaSp2* is driven by the *fibroin heavy chain* promoter, and DsRed2 serves as the selection marker of transgene-positive animals.

Analysis of inverse PCR followed by sequencing confirmed that transgenic cassette was inserted into intergenic region of the genome (Fig. S2D).

Synthesis and secretion of MaSp2 in transformed silkworms

Analysis of quantitative real-time PCR (qRT-PCR) was performed to investigate expression of MaSp2 in the transformed silkworms. The SG of *B. mori* can be divided into three parts: the posterior silk gland (PSG), the middle silk gland (MSG), and the anterior silk gland (ASG) (Fig. 2A). We detected relative mRNA levels of *MaSp2* in the wild type (WT) and the three transformed silkworm lines. *MaSp2* is specifically expressed in the PSG, with the highest expression level in *H-Sp2-R* line, and the lowest expression level in *H-Sp2-T* animals (Fig. 2B). We also performed immunostaining assays for tissue sections of PSG, and results were in accordance with the mRNA levels of MaSp2 in the three lines (Fig. S3). The relative mRNA levels of *MaSp2* increased gradually from the early fifth larval stage to later stage, mimicking the expression pattern of the endogenous *BmFibH* gene (42) (Fig. 2C). In addition, we also detected MaSp2 at protein level in the PSG of transformed silkworm larvae by using SDS–PAGE and Western blotting analyses (Fig. 2D and E). *H-KO* represents the *BmFibH* knocking out line constructed in previous study (39). In *L-Sp2-F* line, MaSp2 protein displayed two specific bands with different molecular weights, attributing to different efficiency of 2A self-cleave peptide. In Western blotting analysis, MaSp2 displayed higher molecular weight than supposed in *H-Sp2-R* and *H-Sp2-T* line, due to extra peptides of NTD and CTD. In SDS–PAGE analysis, the molecular weight of MaSp2 in *H-Sp2-R* line appeared smaller, probably owing to superabundant of MaSp2 protein. We also performed Western blotting analysis in cocoon shells of WT and transformed silkworms and verified that MaSp2 was secreted into cocoons (Fig. 2F). These results suggested that MaSp2 was specifically expressed in the PSG, and successfully secreted into cocoon of transform silkworms.

Physiological characteristics of transformed silkworms

The MaSp2 transformed silkworms grew and developed normally, except for slight decrease of larval weight in *L-Sp2-F* and *H-KO*

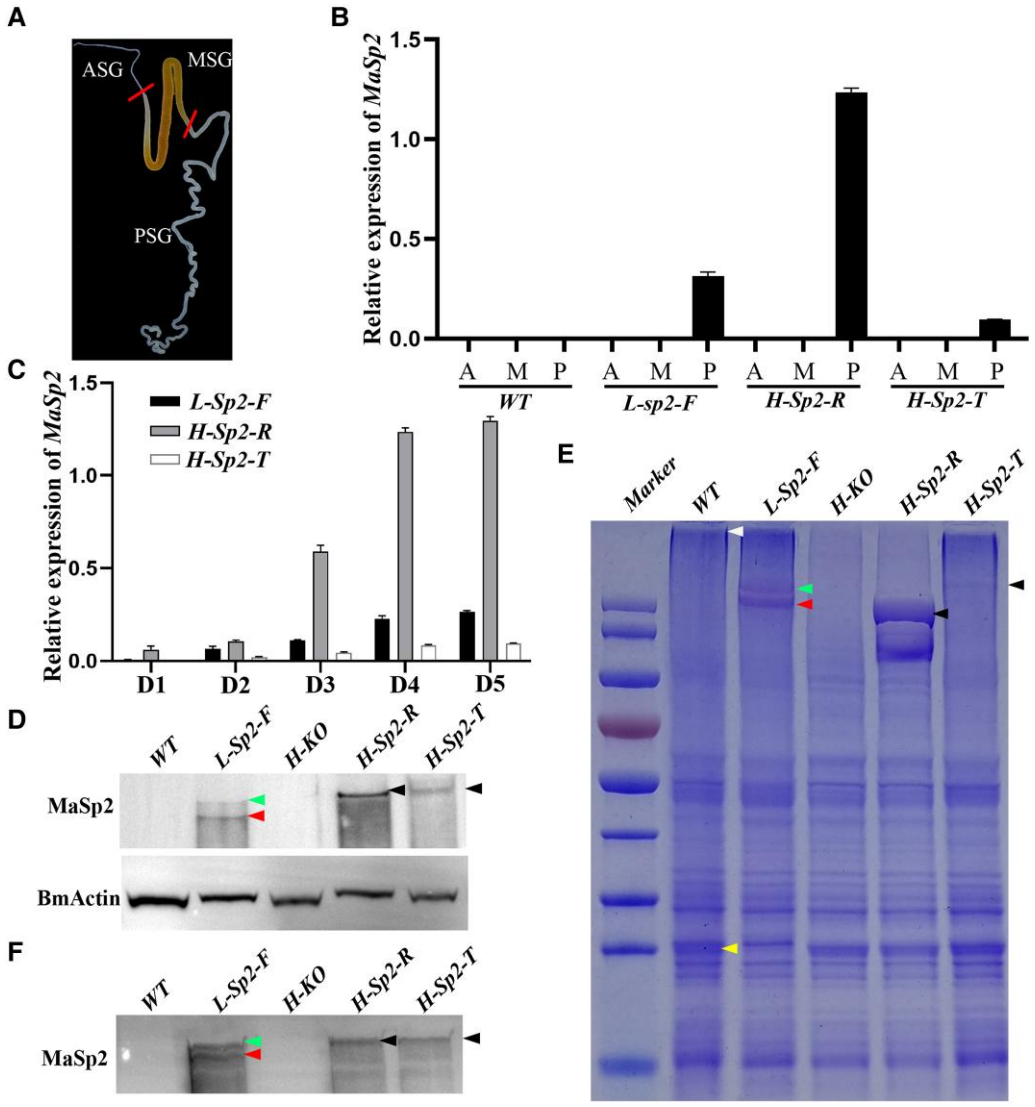

Fig. 2. Synthesis and secretion of MaSp2 in transformed silkworms. A) Representative image of the silkworm SG. B) Relative mRNA level of *MaSp2* in SG of *WT* and transformed silkworms at fourth day of fifth larval stage (L5D4). A, M, and P represent ASG, MSG, and PSG, respectively. C) Relative expression of *MaSp2* in PSG of *WT* and transformed silkworms. D1–D5 represent the first day to fifth day of the fifth larval stage. D) Western blotting analysis of MaSp2 protein in PSG of *WT* and transformed silkworms at L5D4. E) The SDS–PAGE analyses of PSG from *WT* and transformed silkworms. F) Western blotting analysis of MaSp2 protein in cocoon of *WT* and transformed silkworms. Arrows in *L-Sp2-F* lane represent un-cleaved MaSp2 linked with BmFibL and MaSp2 respectively; arrows in *WT* lane represent BmFibH and BmFibL respectively; arrows in *H-Sp2-R* and *H-Sp2-T* lanes signify MaSp2 linked with peptide of NTD and CTD.

lines at the fifth instar larval stage (Fig. S4). The morphology of SG in *H-Sp2-R* and *H-Sp2-T* lines appeared normal, whereas PSG of *L-Sp2-F* silkworms were swollen and crimped (Fig. 3A, top and middle lanes). To investigate the internal structures of PSG, we stained paraffin-embedded tissue sections with hematoxylin and eosin at the fourth day of fifth larval stage. Lumen of PSG in *L-Sp2-F* lines thicken, and the protein secretion was almost completely disordered in *H-KO* line, while in *L-Sp2-F*, *H-Sp2-R*, and *H-Sp2-T* lines, PSGs displayed slight atrophic protein secretion (Fig. 3A, bottom lane). In addition, the length of PSG and weight of SG were sharply decreased in *L-Sp2-F* and *H-KO* line. By contrast, barely reduction was observed in length and weight of PSG in *H-Sp2-R* and *H-Sp2-T* animals (Fig. 3B and C). We next examined the expression levels of endogenous fibroin proteins through qRT-PCR and Western blotting analysis. Expression levels of *BmFibL* and *BmFibH* were sharply decreased in *L-Sp2-F* animals, while barely changed in *H-Sp2-T* animals. In *H-KO* and *H-Sp2-R* animals, expression of *BmFibH* was completely disrupted but expression of *BmFibL* was equivalent to that of *WT* animals (Fig. 3D and E). In all transformed animals, the relative accumulation levels of *BmP25* were comparedwith that of *WT* silkworms (Fig. 3F). Subsequently, we evaluated the commercially important traits of the transformed silkworms. No evident abnormity was observed except for very thin cocoon shells observed in *H-KO* line (Fig. S5A). Both *L-Sp2-F* and *H-KO* lines showed increased pupa weight compared with that of *WT* animals, while the pupa weight in *H-Sp2-R* and *H-Sp2-T* lines were consistent with *WT* silkworms (Fig. S5B and Table S2). However, the weight of the cocoon shells and cocoon shells ratio were significantly decreased in *L-Sp2-F*, *H-KO*, and *H-Sp2-R* lines (Fig. 4A and B). Based on the average weight of each cocoon shell between 28.8 mg for *H-KO* animals and 58.8 mg for *H-Sp2-R* animals, the average MaSp2 protein amount was calculated as 30 mg in each cocoon shell, which reached to 51.02% of total cocoon shell weight in *H-Sp2-R* animals (39).

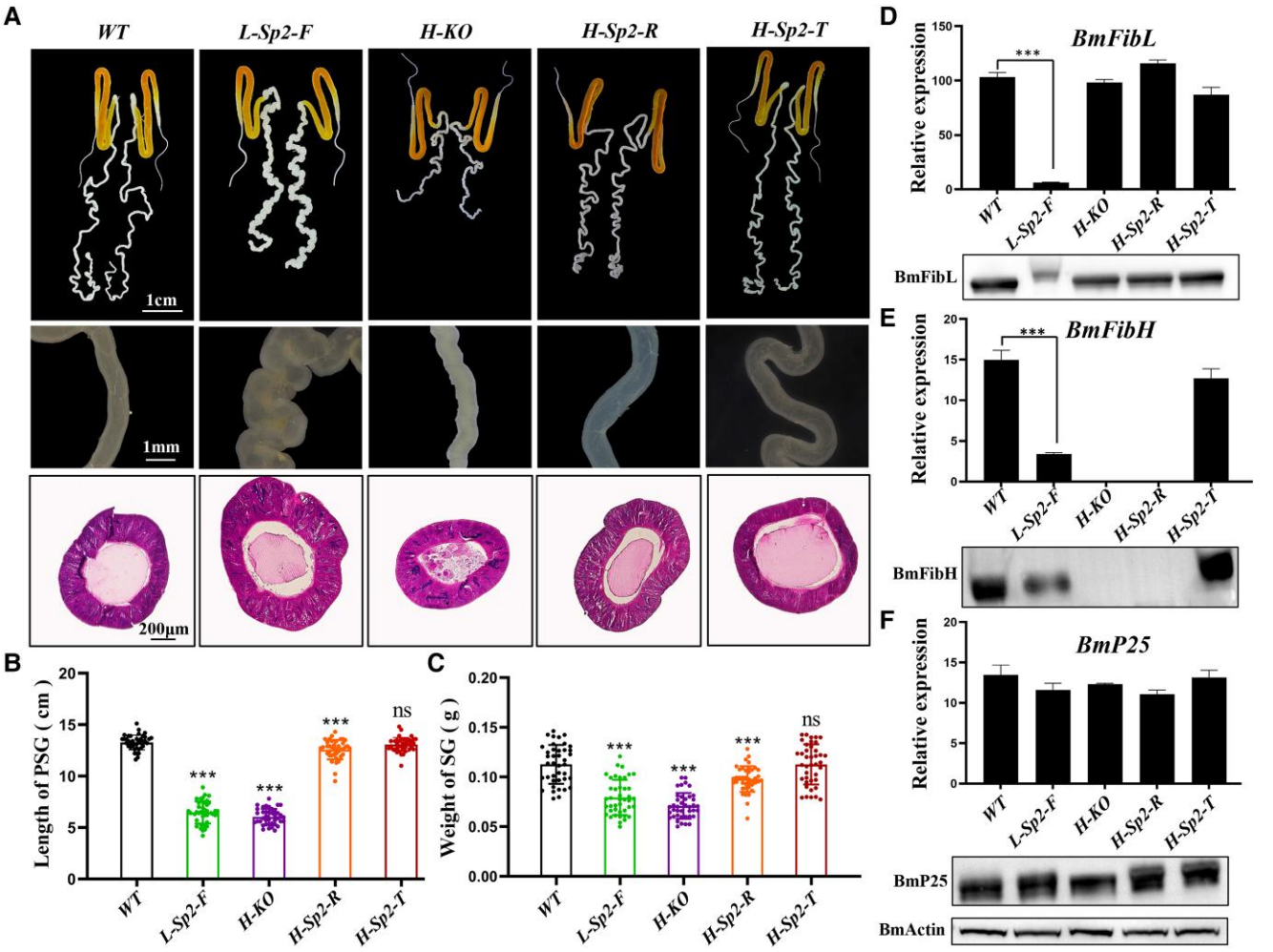

Fig. 3. Physiological characteristics of transformed silkworms. A) Morphological analysis of SG in *WT* and transformed silkworms. Top row, gross morphology of the silk glands. Middle row, PSG of *WT* and transformed silkworms. Bottom row, paraffin-embedded sections of the PSG stained with hematoxylin–eosin. B and C) The statistical analysis of the length of the PSG B) and weight of the intact SG C) ($n = 40$). Error bar: SD; *** represents significant differences at the 0.001 level (t test) compared with the control. D–F) qRT-PCR and Western blotting analysis of BmFibL D), BmFibH E), and BmP25 F).

Transcriptome analysis of transformed silkworms

To further explore the characteristics of different systems, we performed RNA-seq analysis for PSG from *WT* and transformed silkworms at fourth day of fifth larval stage. There were 1,810, 1,352, 212, and 102 differentially expressed genes (DEGs) in *L-Sp2-F*, *H-KO*, *H-Sp2-R*, and *H-Sp2-T* lines, respectively. In addition, KEGG enrichment analysis revealed that DEGs in *L-Sp2-F* line was primarily involved in translation processes such as ribosome, ribosome biogenesis in eukaryotes and spliceosome pathways. In *H-Sp2-R* and *H-Sp2-T* lines, DEGs were also predominantly enriched in translation processes such as alanine, aspartate, and glutamate metabolism, glycine, serine, and threonine metabolism and arginine biosynthesis pathways. Interestingly, DEGs were enriched in protein processing in endoplasmic reticulum pathway in all the three lines (Fig. S6B–D). These results indicated that ectopic expression of exogenous protein would influence endogenous protein biosynthesis in varying degrees, despite that BmFibH-R and BmFibH-T system only resulted in minor impacts.

Existence of MaSp2 enhanced extensibility of silk fibers

We next investigated the mechanical properties of the single silk fibers from transformed silkworms. The average breaking stress, which signifies strength, of *L-Sp2-F* fiber slightly decreased by 9.23% compared with fibers from *WT* animals. In comparisons, the average breaking stress of *H-Sp2-R* and *H-Sp2-T* fiber increased by 12.57 and 33.99% respectively. The average value of Young's modulus showed no significant difference between silk fibers from transformed and *WT* animals. The average breaking strain of silk fibers were significantly improved by 44.73, 55.44, and 47.08% in *L-Sp2-F*, *H-Sp2-R*, and *H-Sp2-T* stains, respectively. Furthermore, the silk fibers from *L-Sp2-F*, *H-Sp2-R*, and *H-Sp2-T* lines showed increased breaking energy, which represents toughness, by 34.86, 73.87, and 86.18%, respectively (Fig. 4C–G and Table S3). These results indicated that existence of MaSp2 can significantly enhance extensibility and toughness of silk fibers.

Expression of chimeric EvFibH improved strength of silk fibers

We next constructed transformed silkworm lines with expression of 226 kDa EvFibH by using BmFibH-T and BmFibH-R systems, considering their minor impact on physiology of the silkworms. The chimeric EvFibH protein consists of 21 repetitive motifs, each of which is composed of polyalanine block (PAB) and nonpolyalanine block (NPAB) sequences. The construction strategies were similar to that of MaSp2 transformation stains (Fig. S7A

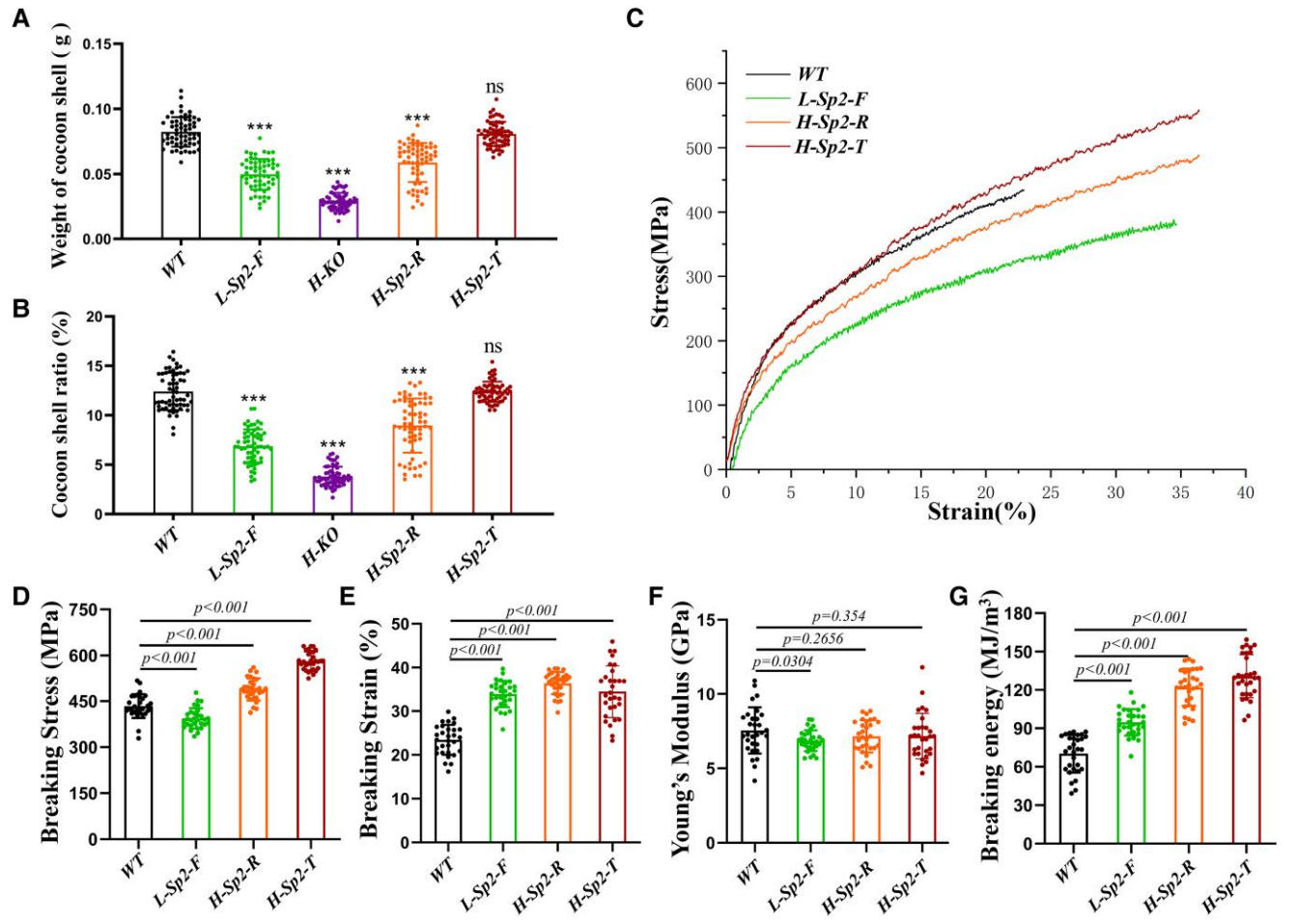

Fig. 4. Existence of MaSp2 can greatly enhance extensibility of silk fibers. A and B) The statistical analysis of the weight of cocoon shell A) and cocoon shell ratio B) ($n = 60$). Error bar: SD; *** represents significant differences at the 0.001 level (t test) compared with the control. C) Stress–strain curves of *WT* and transformed silk fibers. D–G) Mechanical properties including breaking stress D), breaking strain E), Young's modulus F), and breaking energy G) of silk fibers from *WT* and transformed silkworms.

and B). Genotypes of *H-EvFH-T* and *H-EvFH-R* positive animals were examined through inverse PCR and junction PCR, respectively (Fig. S7C and D). For *H-EvFH-R* line, a ~12 kb fragment was precisely integrated in the genome. Both lines grew normally, and no developmental defects appeared (Fig. S8A). The gross morphology, length, and weight of silk glands barely changed in transformed silkworms (Fig. S8B–D). More importantly, the commercially important traits did not show significant differences between transformed silkworm and *WT* animals (Fig. S9A–C and Table S4). We subsequently confirmed the existence of EvFibH in PSG and cocoon shells of transformed silkworms through qRT-PCR and Western blotting analyses (Fig. 5A–C). The qRT-PCR analyses also revealed that expression of *EvFibH* hardly affected the relative mRNA level of endogenous fibroin genes (Fig. S9D–F). The average amount of EvFibH protein in cocoons of *H-EvFH-R* line reached 64.13%, calculated based on the average weight difference between 28.8 mg *H-KO* and 80.3 mg *H-EvFH-R* cocoon shells.

We next examined the mechanical properties of silk fibers from *WT* and transformed silkworms. The results revealed that average breaking stress, Young's modulus, and breaking energy of *H-EvFH-R* fiber increased by 69.66, 90.51, and 80.27%, respectively. In contrast, breaking strains of *H-EvFH-R* and *H-EvFH-T* fibers did not change significantly. However, the average breaking stress, Young's modulus, and breaking energy of silk fiber from *H-EvFH-T* line increased by 31.35, 32.36, and 48.93%, respectively (Fig. 5E–H). The data above indicated that existence of EvFibH significantly improved the strength of silk fibers.

Distinct structural changes in chimeric silk fibers

To gain insight into the mechanisms underlying enhanced mechanical properties, we sought to investigate structural changes in chimeric silk fibers. After degumming, we observed no visible distinctions in the morphology of both the surface and tensile fractured cross-sections between the *WT* and different chimeric silk samples (Fig. 6A–F). This resemblance may emphasize the critical role of the terminal domains of fibroins in controlling protein self-assembly in the SG, as all the chimeric proteins contain intact NTD and CTD from *WT* silkworm fibroin. We next performed wide-angle X-ray diffraction (WAXD) analysis (Fig. 6G and Fig. S10) and the result showed a noticeable increase in crystallinity, ranging from 22 to 43%, in the fibers with novel chimeric heavy chains, including *H-Sp2-R*, *H-Sp2-T*, *H-EvFH-R*, and *H-EvFH-T*, although the sizes of nanocrystalline remain similar (Table S5). Specifically, the crystallinity of *H-EvFH-R* fiber approximates 44%, closely resembling that of natural *E. variegata* bagworm silk at around 45% (31, 32). It is known that both MaSp2 and EvFibH

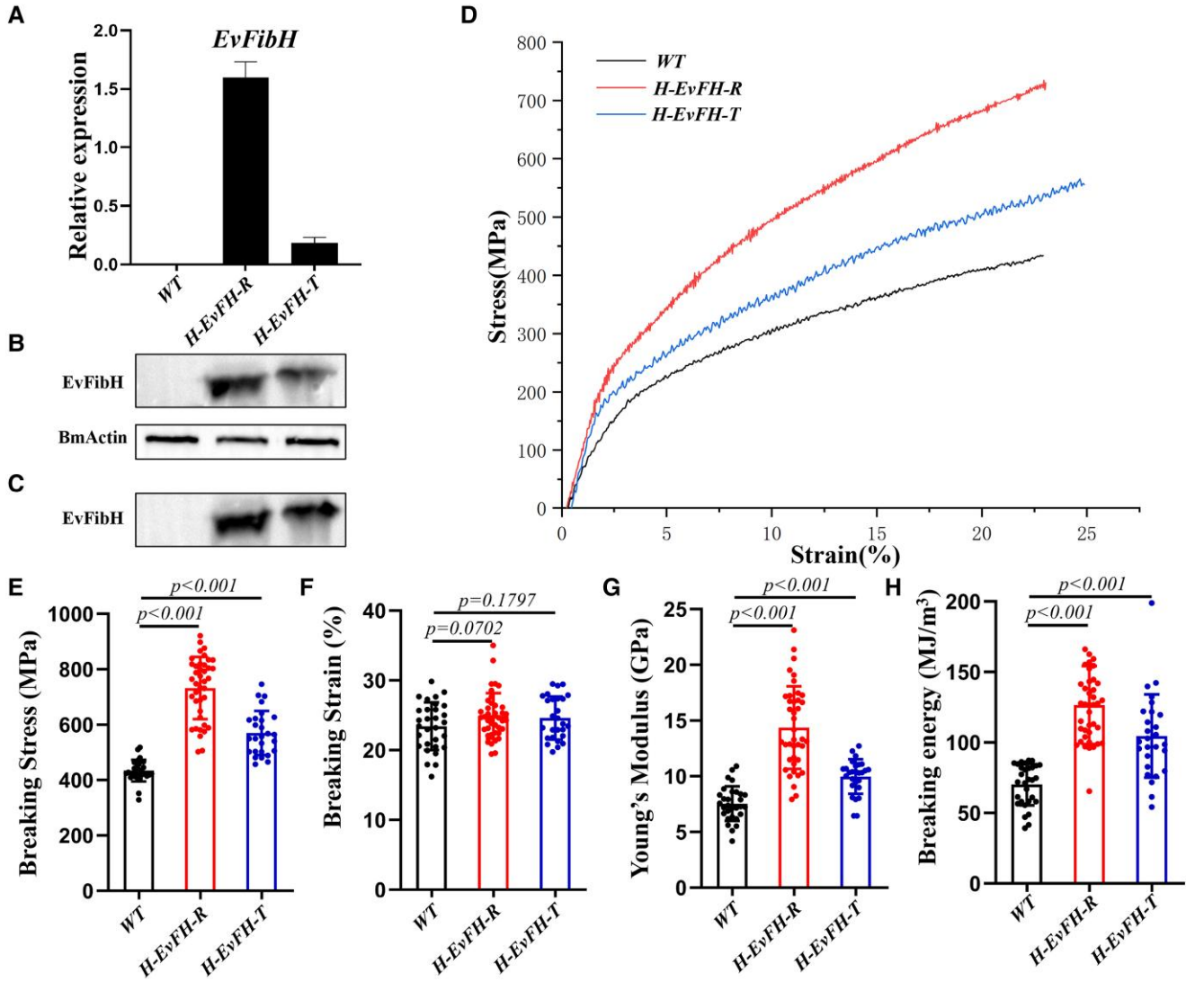

Fig. 5. Existence of chimeric EvFibH can sharply improve comprehensive mechanical performance, especially strength of silk fibers. A) Relative mRNA level of *EvFibH* in SG of *WT* and transformed silkworms at L5D4. B and C) Western blotting analysis of EvFibH protein in PSG B) and cocoon C) of *WT* and transformed silkworms. D) Stress–strain curves of *WT* and transformed silk fibers. E–H) Mechanical properties including breaking stress E), breaking strain F), Young's modulus G), and breaking energy H) of silk fibers from *WT* and transformed silkworms.

repetitive sequences contain polyalanine blocks of varying lengths, typically between 7 and 12 consecutive alanine residues, which are absent in native silkworm fibroins. Therefore, these long polyalanine sequences may be primarily responsible for the formation of more crystalline regions through hydrophobic interactions and contribute to the higher strength and toughness of silks. We further carried out Fourier transform infrared spectroscopy (FTIR) on degummed silk fibers, revealing elevated helical conformation by >20% in chimeric *H-Sp2-R* and *H-Sp2-T* fibers, consistent with their increased plastic deformation capacity and higher extensibility (Fig. 6H and Fig. S11). In addition, we observed that regenerated silk fibroins were rich in similar β-like structures in pure water solution, with the exception of *L-Sp2-F* (Fig. S12). It is conceivable that the presence of the long MaSp2 sequence in the short light chain, due to inefficient self-cleavage, could interfere with the interaction between fibroin heavy and light chains, leading to inhomogeneous fibroin complexes. This may explain the relatively low β-sheet content both in fibroin solution and in spun *L-Sp2-F* fiber with inferior physical properties.

Discussion

In the current study, we achieved ectopic expression of MaSp2 and EvFibH proteins in genetically engineered silkworms by using various expression strategies including BmFibL-F, BmFibH-R, and BmFibH-T systems. In silkworm lines constructed by BmFibH-T system, negligible difference was detected in physiological property compared with that of *WT* animals. The comprehensive mechanical properties of transgenic silkworm fibers were significantly promoted. Nevertheless, the yields of exogenous protein were not so desirable, consistent with previous studies, limiting further improvement of silk mechanical properties (26, 46). We presumed the transgenic system was fit for verifying properties of sequence with particular motifs. By comparison, BmFibL-F system can achieve higher yield of exogenous protein; however, the transformed silkworms displayed evident defects in PSG development and endogenous gene expression. In addition, the comprehensive mechanical properties of fibers from transformed silkworms were not satisfactory compared with other lines, indicating BmFibL-F system is not suitable for improving mechanical properties of silk

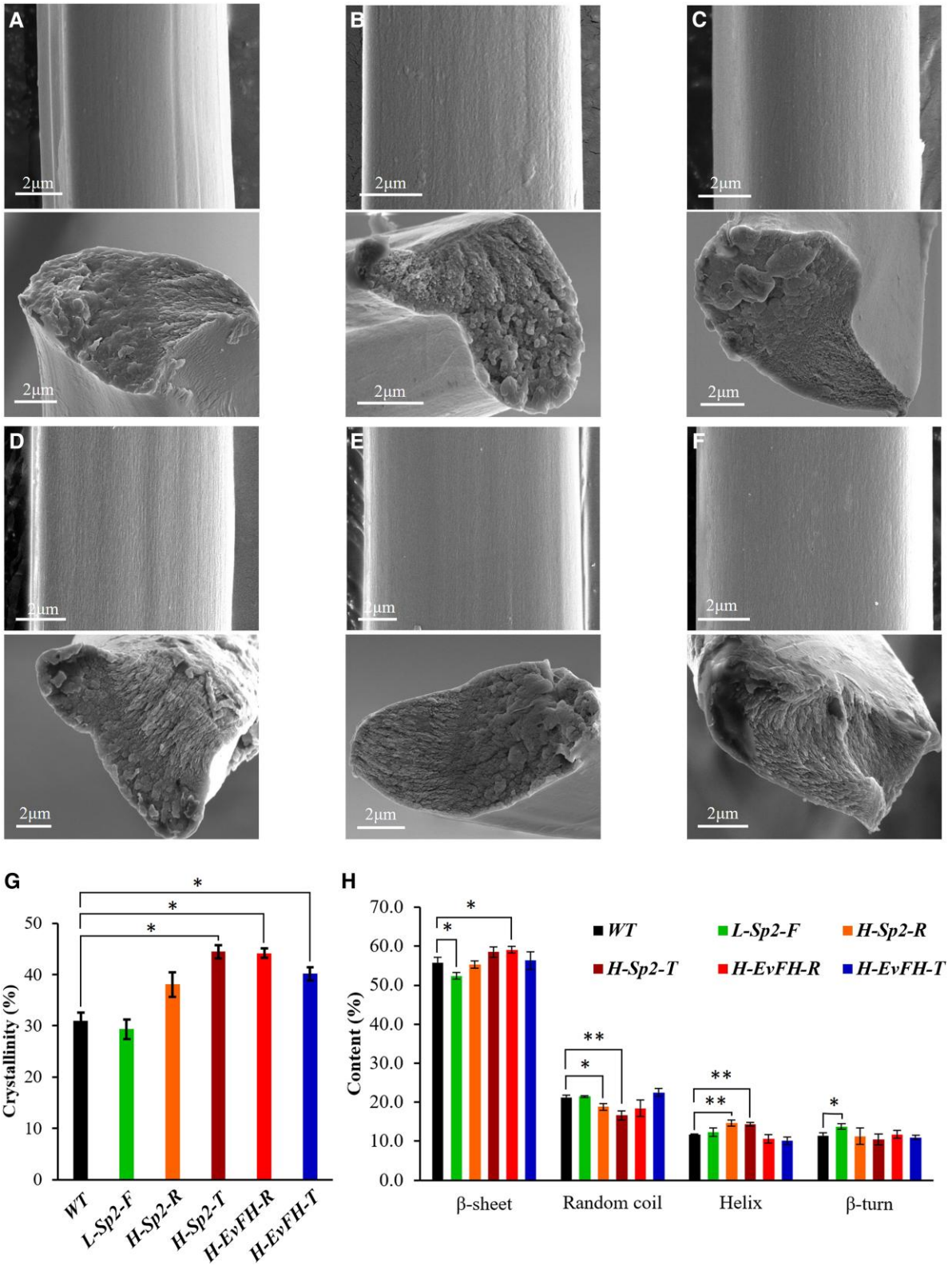

Fig. 6. Characterization of the degummed WT and transformed silkworm silks. A–F) SEM images of surfaces (upper) and cross-sections (lower) of WT A), *L-Sp2-F* B), *H-Sp2-R* C), *H-Sp2-T* D), *H-EvFH-R* E), and *H-EvFH-T* F) silk fibers. Scale bars: 2 μm. G) The crystallinity of the WT and transformed silkworm silks characterized by WAXD. H) Secondary structure content of WT and transformed silkworm silks characterized by FTIR.

fibers. In contrast, the silkworm lines constructed by BmFibH-R system can produce extraordinary amount of exogenous protein with minimal abnormality in physiological properties. More importantly, the mechanical properties of silk fibers from transformed silkworms were drastically improved, suggesting that BmFibH-R system can serve as the ideal strategy. In addition, the

BmFibH-R system can achieve up to 12 kb fragment integration precisely, revealing its tremendous potential for expressing protein with high molecular weight. In our study, the BmFibH-R system achieved expression of a 226 kDa protein, which has higher molecular weight than the 150 kDa minor ampullate spidroin (MiSp) reported in the recent study (43). Compared with the previous study inserting spider silk genes into intron of *BmFibH* and *BmFibL* thorough CRISPR/Cas9 mediated nonhomologous end joining, the BmFibH-R strategy can achieve precise seamless insertion (44). In our study, the efficiency of TALEN-mediated transformation strategy was lower than that of piggyBac-based transgenic system. We speculated this was attributed from multiple insertion sites in *piggyBac*-mediated transformation strategy.

The physical properties of silk fibers are primarily determined by the primary structure and secondary structure of silk protein (7–10). Based on the sequence characteristics, MaSp2 and EvFibH were supposed to be responsible for extensibility and strength of silk fibers, respectively. Nonetheless, mechanical properties of silk fibers cannot be easily explained by the condensed state structures made from diverse motifs. Our study provided experimental evidence that MaSp2 and EvFibH are implicated in extensibility and strength of silk fibers, providing sequence materials for exploiting custom-designed silks. In our previous study, we achieved 67 kDa chimeric MaSp1 protein expression with a yield of 35.2% in a single cocoon shell using the BmFibH-R system. However, it was difficult to obtain single fibers from the cocoon shells of homozygous transformed silkworms, which also showed apparent defects in PSG development, likely being responsible from low molecular weight of MaSp1 compared with that of original 350 kDa BmFibH (39). In the current study, we obtained transformed silkworm lines with the expression of 160 kDa MaSp2 and chimeric 226 kDa EvFibH, two proteins with much higher molecular weight compared with that of MaSp1, by using the BmFibH-R system. Remarkably, the amounts of exogenous proteins can reach 51.02 and 64.13% in cocoon shells of *H-Sp2-R* and *H-EvFH-R* lines, respectively, verifying our previous hypothesis that integrating proteins of higher molecular weights can further increase protein yield. Moreover, mechanical properties of silk fibers from the homozygous transformed silkworms, especially *H-EvFH-R* line, were vastly enhanced. In addition, the higher molecular weight of integrated protein appeared to alleviate the unfavorable consequence caused by BmFibH deletion on SG development. It is worth mentioning that the comprehensive mechanical performance of *H-EvFH-R* fiber is much better than that of *H-EvFH-T* line. By comparison, fiber of *H-Sp2-T* line displayed better mechanical properties than that of *H-Sp2-R* line, indicating that higher content of exogenous protein with higher molecular weight can further promote mechanical properties of silk fibers. In this study, chimeric EvFibH protein consists of 21 repetitive motifs, we speculated the mechanical properties of silk fibers and yield of protein can be further improved when increasing repetition times of the motifs.

Numerous studies have been attempted to promote mechanical properties of silk fibers through expression exogenous proteins, notably spider silk proteins. Nonetheless, the majority of studies were restricted to the expression of one kind of protein with certain physical properties, such as extensibility, strength, or stickiness (26, 43, 44, 46–49). Future clarifying relationship between the sequence structure and physical properties of silk proteins will be useful for integrating chimeric proteins combining with multiple characteristic motifs. Overall, our study provides the ideal strategy for exploiting custom-designed, mass silk production in genetically modified silkworms.

Materials and methods

Silkworm material and growth conditions

We used Nistari, a multivoltine, nondiapausing silkworm strain, for all experiments. Larvae were reared on fresh mulberry leaves under standard conditions (45).

Plasmids construction

The protein sequence of MaSp2 was downloaded from the National Center for Biotechnology Information (NCBI), and the GenBank accession number is AF350276. The chimeric EvFibH protein consists of 21 repetitive motifs, each of which is composed of PAB and NPAB sequences. The nonrepetitive NTD and CTD sequence was removed from original sequence, which was downloaded from NCBI, and the GenBank accession number is GBP83862.1. The CDSs were then optimized for better protein expression in *B. mori* and synthesized commercially by Sangon Biotech (Shanghai, China). For plasmid donors used in BmFibH replacement system, the plasmids construction methods were described previously (39). Briefly, CDSs of *MaSp2* and *EvFibH* were subcloned into the PJTE-1.2-L-arm-3 × P3-dsRed2-R-arm vector to form PJTE-1.2-L-arm-MaSp2-3 × P3-dsRed2-R-arm (*BmFibH-MaSp2*-Donor) and PJTE-1.2-L-arm-EvFibH-3 × P3-dsRed2-R-arm (*BmFibH-EvFibH*-Donor), respectively. As for BmFibL fusion system, the DNA fragments ~1 kb in length each that are homologous to the BmFibL locus immediately adjacent to the 5′ and 3′ ends of the TALEN cleaving site and 3 × P3-dsRed2 cassette were subcloned into PJET-1.2 vector (Invitrogen) to generate PJTE-1.2-FibL-L-arm-3 × P3-dsRed2-FibL-R-arm plasmid. The CDS of *MaSp2* with 2A self-cleaving peptide at 5′ end was subcloned into the former plasmid to form PJTE-1.2-FibL-L-arm-2A-MaSp2-3 × P3-dsRed2-FibL-R-arm (*FibL-MaSp2*-Donor). For *piggyBac*-mediated BmFibH transgenic system, CDSs of *MaSp2* and *EvFibH* were subcloned into pBac-3 × P3-dsRed2 vector to form pBac-3 × P3-dsRed2-FibH-P-NTD-MaSp2-CTD (*FibH-MaSp2* Transgenic plasmid) and pBac-3 × P3-dsRed2-FibH-P-NTD-EvFibH-CTD (*FibH-EvFibH* Transgenic plasmid), respectively. The composition of NTD and CTD was described previously (39, 42).

Germline transformation

For BmFibL fusion system and BmFibH replacement system, the mixture of donor plasmid (250 ng/μL) and TALEN mRNAs (300 ng/μL for each) were microinjected into preblastoderm embryos (G_0 embryos). For piggyBac-mediated FibH transgenic system, a mixture of transformation expression plasmids (400 ng/μL) and helper plasmids (200 ng/μL) were microinjected into G_0 embryos (33). All treatments were completed within 8 h after oviposition. Injected embryos then were incubated at 25°C in a humidified chamber for ~10 days until larvae hatched. The G_0 larvae were reared to the adult stage and mated to *WT* moths. G_1 progeny were screened for the presence of the fluorescent marker using a Nikon SMZ1270 fluorescence microscope.

Quantitative real-time PCR (qRT-PCR)

qRT-PCR analyses were performed using SYBR Green Real-time PCR Master Mix (TOYOBO). Fluorescence signals were recorded using the CFX connect qRT-PCR instrument (Bio-Rad). PCR conditions were those given in the instructions for use of SYBR Green Real-time PCR Master Mix. *Bombyx mori ribosomal protein 49* (*rp49*) was used as internal reference. Three independent biological replicates were performed for each qRT-PCR analysis. All oligonucleotide primers are listed in Table S7.

Paraffin sectioning and hematoxylin–eosin staining

PSGs of transformed and WT animals were dissected from the larvae at fourth day of fifth larval stage and prefixed with Qurnah's fixative (anhydrous ethanol:acetic acid:chloroform, 6:1:3 [v/v/v]) for 24 h. Samples were dehydrated using anhydrous ethanol for 3 times (1 h per time), followed by clearing for 3 times (10 min per time) using xylene. Tissues were embedded in paraffin overnight and were cut into cross-sections (5 μm) with a Leica HistoCore BIOCUT microtome. The sections were rehydrated and then stained using a mixture of hematoxylin and eosin (Beyotime, Shanghai) to visualize morphology. The stained sections were photographed by using an Olympus BX53 microscope.

Immunostaining of PSGs

The paraffin-embedded sections of PSG were firstly rehydrated by steps as follow: xylene for twice, 10 min per time, 95% ethanol for twice, 5 min per time, 80% ethanol for 5 min, 70% ethanol for 5 min, H_2O for twice, 3 min per time, followed by phosphate buffered saline (PBS) for 5 min. Sections were treated with 0.1% trisodium citrate containing 0.1% Triton X-100 for 20 min at 95°C for antigen retrieval. The samples were washed using PBS for twice, followed by blocking with 1% bovine serum albumin for 1 h at room temperature. The sections were then incubated with primary antibodies for 48 h at 4°C. Primary antibodies used for immunostaining were as follows: polyclonal rabbit anti-MaSp2 (1:200), polyclonal rabbit anti-BmFibH (1:200). The samples were washed with PBS for 3 times and incubated with Cy3 goat antirabbit IgG (H + L) (1:1,000) secondary antibody (ABclonal) for 2 h at room temperature. The samples were washed for once and treated with Hoechst33258 for 10 min at room temperature. The samples were washed for 6 times and analyzed with a Nikon C2 Confocal Laser Scanning Microscope.

RNA-seq analysis

For each sample in each silkworm line, total RNA was extracted from PSGs of three larvae at fourth day of fifth larval stage. Samples were treated with DNaseI to avoid genomic DNA contamination, purified, and dissolved in UltraPure distilled water (Invitrogen). The integrity of total RNA was confirmed using agarose electrophoresis, and 20 μg of each sample was sequenced (OE Biotech, Shanghai). For each group, three individual biological replicates were performed. The genes differentially expressed in WT animals and transformed silkworms were identified. KEGG pathway analyses were applied to identify pathways altered in the transformed silkworms.

Mechanical testing of silk fibers

Single silk fibers of the WT and transformed silkworms were subjected to mechanical tests. The sericin layer of silk fibers was removed by gentle stirring in 0.05% (wt/vol) $NaHCO_3$ for 30 min at 100 °C. The degummed silk fibers were washed with water at 80–90 °C with careful stirring followed by distilled water washing at room temperature for 6 times. Individual fibers were tested for breaking stress, breaking strain, Young's modulus, and breaking energy. The cross-sectional areas for fibers were determined by taking an average of 15 measurements using a freezing microtome and confocal microscopy (Nikon C2). Single-fiber testing was performed with the MTS C42 mechanical testing instrument (at 20–25 °C and 40–45% relative humidity; gauge length: 20 mm; crosshead speed: 5 mm/min) with a cell load of 5 N. Each group has at least 45 fibers derived from five different individual cocoons.

Preparation of WT and transformed silkworm fibroins

The WT and transformed silkworm cocoons were degummed in 0.25% (w/v) SDS and 0.25% (w/v) Na_2CO_3 solution at 80 ± 2°C for 5 min (50). The silks were then washed thoroughly in deionized water and dried at 55 °C. Fully dried silks were weighted and then vortexed and shaken in 9.8 M LiBr until they were nearly completely dissolved. After centrifugation, the supernatant was dialyzed against deionized water and diluted to obtain fibroin solutions with a concentration of ∼1.2 mg/mL for circular dichroism (CD) experiments.

Scanning electron microscope

The surface and the cross-section of the WT and transformed silkworm silks were observed with an Apreo S LoVac field emission scanning electron microscopy at 5 kV after sputtering with gold.

CD measurement

The secondary structures of WT and transformed silkworm fibroins were determined by CD spectra measured using a Biotools MOS-500 spectrometer under a nitrogen atmosphere at room temperature. All spectra were recorded between 260 and 190 nm with three scans accumulated.

Fourier transform infrared spectroscopy

WT and transformed silkworm cocoons degummed with boiled 0.5% (w/v) $NaHCO_3$ for 30 min were used for testing FTIR and XRD. Undegummed WT silk was prepared from cocoons in hot pure water. FTIR studies were performed using a Thermo Nicolet IN10 microscopic infrared spectrometer equipped with a deuterated triglycine sulfate detector and an attenuated total reflection attachment. All spectra were scanned within the range of 400–4,000 cm^{-1} and a resolution of 8 cm^{-1}. All FTIR spectra were deconvoluted using Origin 2018. The secondary structure content of the fiber was calculated by the ratio of the peak area of the corresponding peak position (51).

Wide-angle X-ray diffraction

The X-ray diffraction patterns of the WT and transformed silkworm silks were collected by a Rigaku D/Max 2500 X-ray diffractometer with CuKα radiation (λ = 0.154 nm) at a generator of 40 kV and a current of 200 mA with the angle range of 3°–60°. The scanning speed was 4° min^{-1} with a scanning step of 0.02°. MDI Jade 6.5 was used to analyze all diffraction patterns. The crystallinity is the ratio of the crystal peaks area to the total area, and the crystalline sizes of the two (020) and (200)/(210) reflections were calculated according to Scherrer formula (52).

Statistics

Experimental data were analyzed with the Student's t test using GraphPad Prism 8 software. The asterisks indicate different *P*–value: *, $P < 0.05$; **, $P < 0.01$; ***, $P < 0.001$.

Supplementary Material

Supplementary material is available at *PNAS Nexus* online.

Funding

This work was supported by the National Natural Science Foundation of China (grant no. 31925007 to A.T., 32102611 to K.C.) and the Natural Science Foundation of Jiangsu Province (grant no. BK20210880 to K.C.).

Author Contributions

Y.Y., K.C., L.Z., and A.T. designed research; Y.Y., K.C., and J.W. performed research; K.C., Y.Y., and J.W. contributed analytic tools; K.C., Y.Y., Z.Z., B.H., X.L., and A.T. analyzed data; and K.C., L.Z., and A.T. wrote the paper.

Data Availability

The RNA-seq raw data in this study have been deposited in NCBI SRA database (https://submit.ncbi.nlm.nih.gov/subs/sra/) with accession numbers SRR26898930–SRR26898947. All data needed to evaluate the conclusions in the paper are present in the paper and/or the supplementary material.

References

1 Kluge JA, Rabotyagova O, Leisk GG, Kaplan DL. 2008. Spider silks and their applications. *Trends Biotechnol*. 26:244–251.
2 Craig CL. 1997. Evolution of arthropod silks. *Annu Rev Entomol*. 42: 231–267.
3 Parent LR, *et al*. 2018. Hierarchical spidroin micellar nanoparticles as the fundamental precursors of spider silks. *Proc Natl Acad Sci U S A*. 115:11507–11512.
4 Wang Y, Ren J, Ye C, Pei Y, Ling S. 2021. Thermochromic silks for temperature management and dynamic textile displays. *Nanomicro Lett*. 13:72.
5 Gong Z, *et al*. 2021. Upconversion nanoparticle decorated spider silks as single-cell thermometers. *Nano Lett*. 21:1469–1476.
6 Sutherland TD, Young JH, Weisman S, Hayashi CY, Merritt DJ. 2010. Insect silk: one name, many materials. *Annu Rev Entomol*. 55:171–188.
7 Huang W, Ling S, Li C, Omenetto FG, Kaplan DL. 2018. Silkworm silk-based materials and devices generated using bio-nanotechnology. *Chem Soc Rev*. 47:6486–6504.
8 Adrianos SL, *et al*. 2013. *Nephila clavipes* flagelliform silk-like GGX motifs contribute to extensibility and spacer motifs contribute to strength in synthetic spider silk fibers. *Biomacromolecules*. 14: 1751–1760.
9 Tokareva O, Jacobsen M, Buehler M, Wong J, Kaplan DL. 2014. Structure–function–property–design interplay in biopolymers: spider silk. *Acta Biomater*. 10:1612–1626.
10 Rising A, Harrington MJ. 2023. Biological materials processing: time-tested tricks for sustainable fiber fabrication. *Chem Rev*. 123:2155–2199.
11 Huang W, *et al*. 2017. Synergistic integration of experimental and simulation approaches for the de Novo design of silk-based materials. *Acc Chem Res*. 50:866–876.
12 Liu D, *et al*. 2019. Spider dragline silk as torsional actuator driven by humidity. *Sci Adv*. 5:eaau9183.
13 Malay AD, Craig HC, Chen J, Oktaviani NA, Numata K. 2022. Complexity of spider dragline silk. *Biomacromolecules*. 23:1827–1840.
14 Wong Po Foo C, Kaplan DL. 2002. Genetic engineering of fibrous proteins: spider dragline silk and collagen. *Adv Drug Deliv Rev*. 54:1131–1143.
15 Kono N, *et al*. 2021. Multicomponent nature underlies the extraordinary mechanical properties of spider dragline silk. *Proc Natl Acad Sci U S A*. 118:e2107065118.
16 Humenik M, Scheibel T, Smith A. 2011. Spider silk: understanding the structure-function relationship of a natural fiber. *Prog Mol Biol Transl Sci*. 103:131–185.
17 Heim M, Keerl D, Scheibel T. 2009. Spider silk: from soluble protein to extraordinary fiber. *Angew Chem Int Ed Engl*. 48:3584–3596.
18 Blamires SJ, Blackledge TA, Tso IM. 2017. Physicochemical property variation in spider silk: ecology, evolution, and synthetic production. *Annu Rev Entomol*. 62:443–460.
19 Sponner A, Unger E, Grosse F, Weisshart K. 2005. Differential polymerization of the two main protein components of dragline silk during fibre spinning. *Nat Mater*. 4:772–775.
20 Arndt T, *et al*. 2022. Engineered spider silk proteins for biomimetic spinning of fibers with toughness equal to dragline silks. *Adv Funct Mater*. 32:2200986.
21 Blamires SJ, Wu CC, Wu CL, Sheu HS, Tso IM. 2013. Uncovering spider silk nanocrystalline variations that facilitate wind-induced mechanical property changes. *Biomacromolecules*. 14: 3484–3490.
22 Santos-Pinto JR, Arcuri HA, Lubec G, Palma MS. 2016. Structural characterization of the major ampullate silk spidroin-2 protein produced by the spider *Nephila clavipes*. *Biochim Biophys Acta*. 1864:1444–1454.
23 Brooks AE, *et al*. 2008. Properties of synthetic spider silk fibers based on *Argiope aurantia* MaSp2. *Biomacromolecules*. 9:1506–1510.
24 Dos Santos-Pinto JRA, Arcuri HA, Esteves FG, Palma MS, Lubec G. 2018. Spider silk proteome provides insight into the structural characterization of *Nephila clavipes* flagelliform spidroin. *Sci Rep*. 8:14674.
25 Htut KZ, *et al*. 2021. Correlation between protein secondary structure and mechanical performance for the ultra-tough dragline silk of Darwin's bark spider. *J R Soc Interface*. 18:20210320.
26 Teulé F, *et al*. 2012. Silkworms transformed with chimeric silkworm/spider silk genes spin composite silk fibers with improved mechanical properties. *Proc Natl Acad Sci U S A*. 109:923–928.
27 Cao H, *et al*. 2017. Metabolic engineering for recombinant major ampullate spidroin 2 (MaSp2) synthesis in *Escherichia coli*. *Sci Rep*. 7:11365.
28 Brooks AE, *et al*. 2008. Distinct contributions of model MaSp1 and MaSp2 like peptides to the mechanical properties of synthetic major ampullate silk fibers as revealed in silico. *Nanotechnol Sci Appl*. 1:9–16.
29 Rhainds M, Davis DR, Price PW. 2009. Bionomics of bagworms (Lepidoptera: Psychidae). *Annu Rev Entomol*. 54:209–226.
30 Kono N, Nakamura H, Tateishi A, Numata K, Arakawa K. 2021. The balance of crystalline and amorphous regions in the fibroin structure underpins the tensile strength of bagworm silk. *Zoological Lett*. 7:11.
31 Kono N, *et al*. 2019. The bagworm genome reveals a unique fibroin gene that provides high tensile strength. *Commun Biol*. 2: 148.
32 Yoshioka T, Tsubota T, Tashiro K, Jouraku A, Kameda T. 2019. A study of the extraordinarily strong and tough silk produced by bagworms. *Nat Commun*. 10:1469.
33 Garb JE, *et al*. 2019. The transcriptome of Darwin's bark spider silk glands predicts proteins contributing to dragline silk toughness. *Commun Biol*. 2:275.
34 Kono N, *et al*. 2021. Darwin's bark spider shares a spidroin repertoire with *Caerostris extrusa* but achieves extraordinary silk toughness through gene expression. *Open Biol*. 11:210242.
35 Wolff JO, *et al*. 2017. Strength of silk attachment to *Ilex chinensis* leaves in the tea bagworm *Eumeta minuscula* (Lepidoptera, Psychidae). *J R Soc Interface*. 14:20170007. https://doi.org/10.1098/rsif.2017.0007
36 Tsubota T, *et al*. 2021. Transcriptomic analysis of the bagworm moth silk gland reveals a number of silk genes conserved within Lepidoptera. *Insect Sci*. 28:885–900.
37 Goldsmith MR, Shimada T, Abe H. 2005. The genetics and genomics of the silkworm, *Bombyx mori*. *Annu Rev Entomol*. 50:71–100.

38 Xia Q, Li S, Feng Q. 2014. Advances in silkworm studies accelerated by the genome sequencing of *Bombyx mori*. *Annu Rev Entomol*. 59:513–536.
39 Xu J, *et al.* 2018. Mass spider silk production through targeted gene replacement in *Bombyx mori*. *Proc Natl Acad Sci U S A*. 115: 8757–8762.
40 Otsuki R, *et al.* 2017. Bioengineered silkworms with butterfly cytotoxin-modified silk glands produce sericin cocoons with a utility for a new biomaterial. *Proc Natl Acad Sci U S A*. 114: 6740–6745.
41 Zhang Z, *et al.* 2018. Silkworm genetic sexing through W chromosome-linked, targeted gene integration. *Proc Natl Acad Sci U S A*. 115:8752–8756.
42 Chen K, *et al.* 2023. Engineering a complex, multiple enzyme-mediated synthesis of natural plant pigments in the silkworm, *Bombyx mori*. *Proc Natl Acad Sci U S A*. 120:e2306322120.
43 Mi J, *et al.* 2023. High-strength and ultra-tough whole spider silk fibers spun from transgenic silkworms. *Matter*. 6:3661–3683.
44 Zhang X, *et al.* 2019. CRISPR/cas9 initiated transgenic silkworms as a natural spinner of spider silk. *Biomacromolecules*. 20: 2252–2264.
45 Tan A, *et al.* 2013. Transgene-based, female-specific lethality system for genetic sexing of the silkworm, *Bombyx mori*. *Proc Natl Acad Sci U S A*. 110:6766–6770.
46 Kuwana Y, Sezutsu H, Nakajima K, Tamada Y, Kojima K. 2014. High-toughness silk produced by a transgenic silkworm expressing spider (*Araneus ventricosus*) dragline silk protein. *PLoS One*. 9: e105325.
47 You Z, *et al.* 2018. Extraordinary mechanical properties of composite silk through hereditable transgenic silkworm expressing recombinant major ampullate spidroin. *Sci Rep*. 8:15956.
48 Wen H, *et al.* 2010. Transgenic silkworms (*Bombyx mori*) produce recombinant spider dragline silk in cocoons. *Mol Biol Rep*. 37: 1815–1821.
49 Zhu Z, *et al.* 2010. Mechanical properties of regenerated *Bombyx mori* silk fibers and recombinant silk fibers produced by transgenic silkworms. *J Biomater Sci Polym Ed*. 21:395–411.
50 Ha SW, Tonelli AE, Hudson SM. 2005. Structural studies of *Bombyx mori* silk fibroin during regeneration from solutions and wet fiber spinning. *Biomacromolecules*. 6:1722–1731.
51 Wang J, *et al.* 2022. Artificial superstrong silkworm silk surpasses natural spider silks. *Matter*. 5:4396–4406.
52 Drummy LF, Farmer BL, Naik RR. 2007. Correlation of the β-sheet crystal size in silk fibers with the protein amino acid sequence. *Soft matter*. 3:877–882.